Cross-Facility Comparison of Time-Resolved Ion Energy in the SPT-50 Hall Thruster

IEPC-2025-176

Presented at the 39th International Electric Propulsion Conference Imperial College London • London, United Kingdom 14-19 September 2025

Austen Thomas¹ and Kristina Lemmer²
Western Michigan University, Kalamazoo, MI, 49008, USA
Seth Thompson³ and John Williams⁴
Colorado State University, Fort Collins, CO, 80521, USA

ana

Lee Johnson⁵

Jet Propulsion Laboratory, California Institute of Technology, Pasadena, CA, 91109, USA

Abstract: A facility characterization study was conducted to quantify the impact of facility conditions on Hall effect thruster (HET) operation and support the development of predictive engineering models (PEMs). A 300-W HET was tested at three vacuum facilities, with discharge telemetry and plume property measurements performed at multiple spatial positions and operating conditions. Variations in discharge telemetry and plume property measurements were observed across facilities due to pressure and electrical facility effects. Discharge current mean, peak-to-peak oscillation amplitude, and stability showed significant variations across facilities. Several temporal characteristics of the time-resolved ion energy measurements varied between facilities, including peak-to-peak ion energy oscillations, waveform structure, and the presence of additional ion energy populations. The collected data are being incorporated into the initial development of HET PEM.

⁵ Space Systems Technologist, Electric Propulsion Group, lee.k.johnson@jpl.nasa.gov



¹ PhD candidate, Mechanical & Aerospace Engineering, austen.j.thomas@wmich.edu

² Professor, Mechanical & Aerospace Engineering, kristina.lemmer@wmich.edu

³ PhD candidate, Mechanical & Aerospace Engineering, Seth.Thompson@colostate.edu

⁴ Professor, Mechanical & Aerospace Engineering, John.D.Williams@colostate.edu

Nomenclature

A = Aperture area E_{i-avg} = Average ion energy E_{i-p2p} = Peak-to-peak ion energy e = Elementary charge f = Distribution function

 f_{BM} = Breathing mode fundamental frequency

 I_{coll} = Collector current

 I_{d-avg} = Average discharge current I_{d-p2p} = Peak-to-peak discharge current

 m_i = Ion mass

 T_e = Electron temperature V_{bias} = Retarding potential V_p = Plasma potential θ = Scattering angle

I. Introduction

Electric propulsion (EP) research has been increasingly focused on high-power Hall effect thruster (HET) operation, a focus that presents considerable hurdles. As HETs continue to climb in power, a significant challenge facing ground-based testing of higher-power thrusters is that data collected during ground testing may no longer be indicative of operation in-space. Therefore, predictive engineering models (PEMs) will be required to augment or potentially replace expensive and time-consuming ground testing. As new limits in power and propellant flow are reached, even the most capable vacuum facilities will encounter extreme facility effects, which at present are not predicted by engineering models [1].

The Joint AdvaNced PropUlsion InStitute (JANUS), a NASA Space Technology Research Institute (STRI), is developing these PEMs to predict and account for these extreme facility effects [2]. These models require experimental measurements from high-power EP ground-based tests for their validation and calibration [1, 3]. The goal of JANUS is to incorporate these facility effects and accurately predict the lifetime and performance of in-space high-power EP thrusters using engineering models. Testing higher-power EP thrusters presents challenges, as facility effects increasingly affect thruster operation as power and flow rate increase. An alternative approach to operating high-power EP systems to inform PEMs on extreme facility effects is to operate lower-power systems in a variety of vacuum facilities with differing pumping capacities and sizes. Data from these experiments can potentially be extrapolated to higher-powered systems operating in more capable vacuum facilities. Accurate calibration of HET PEMs necessitates comprehensive plasma diagnostic measurements of the HET exhaust plume, and calibrating the PEMs requires both time-averaged and time-resolved data to fully characterize thruster operation.

Time-averaged plasma diagnostics provide useful insight into HET performance; however, the dynamic nature of these thrusters necessitates time-resolved measurements to capture the temporal behavior critical to their operation. Several diagnostic methods have been developed to measure the temporal characteristics of an EP plasma, including high-speed dual Langmuir probes (HDLPs), time-resolved laser-induced fluorescence (TRLIF), and high-speed retarding potential analyzers (HSRPAs) [4–9]. These diagnostics provide insight into the underlying mechanisms that drive the complex dynamic behavior of HETs, such as the breathing mode, spoke mode, axial transit time oscillations, and the electron drift instability, all of which can influence the performance and operation of HETs [10]. Plasma diagnostics provide an effective means to understand thruster behavior. When these data are combined with measurements of discharge telemetry, a more complete picture of the internal thruster physics can be obtained. In this work, a low-power HET was tested in three vacuum facilities where time resolved and time averaged ion energy and plasma potential were measured in the HET plume. These data long with recorded telemetry are expected to be used to informing PEMs on the evolution of time-resolved plume properties and discharge characteristics.



II. Experimental Setup

A. Thruster

Testing was conducted using the SPT-50, a 300-W HET with a 50-mm-external diameter channel, developed by the Research Institute of Applied Mechanics and Electrodynamics of Moscow Aviation Institute [11, 12]. An

externally mounted, heaterless hollow cathode with a 0.51-mm orifice. provided by Plasma Controls, LLC, was used as the electron source for the SPT-50. For this work, the SPT-50 was operated on Xenon at discharge voltages of 200 V, 250 V, and 300 V. The SPT-50 was operated at the 200-V-operating condition at all three facilities; however, the 250-V and 300-V-conditions were only able to be tested at select facilities as discussed in Section III. The thruster is shown operating in Fig. 1 at the 200-V-condition. In all of the vacuum test facilities, the thruster was mounted along the central axis of the vacuum chamber and fired downstream toward the diagnostics. The anode and cathode flow rates were held at 12 sccm and 2.4 sccm, respectively, and the inner and outer magnetic coils were supplied with 2 A and 4 A, respectively. The thruster body remained electrically connected to cathode common throughout testing. To monitor the thruster's discharge telemetry, high-speed current and voltage probes, unique to each testing facility, were used. All highspeed telemetry data were sampled at rates ranging between 50 - 1000 MS/s by a 12 or 16-bit digitizer.



Figure

B. Facilities

Testing of the SPT-50 was completed in three facilities of varying size, pumping capability, and electrical configuration. These facilities are located at Western Michigan University (WMU) in Kalamazoo, MI, the NASA Jet Propulsion Laboratory (JPL) in Pasadena, CA, and Colorado State University (CSU) in Fort Collins, CO. These facilities are pictured in Fig. 2. Each facility possessed unique instrumentation and equipment, including flow controls, power supplies, ion gauges, and thruster telemetry probes which were used to operate and monitor the thruster. A summary of facility geometry, operating pressure, and discharge filter type is presented in Table 1.

Table 1. Vacuum chamber specifications

Location	Chamber	Diameter (m)	Length (m)	Background pressure (Torr-Xe)	Discharge Filter
WMU	CERES	1.0	1.75	2.4 E-4	LC filter L = 2.5 mH $C = 47 \mu\text{F}$
JPL	Big Green	2.0	4.5	2.5 E-5	N/A
CSU	Orion	1.5	4.6	2.0 E-5	RC Filter $R = 0.1 \Omega$ $C = 10 \mu F$



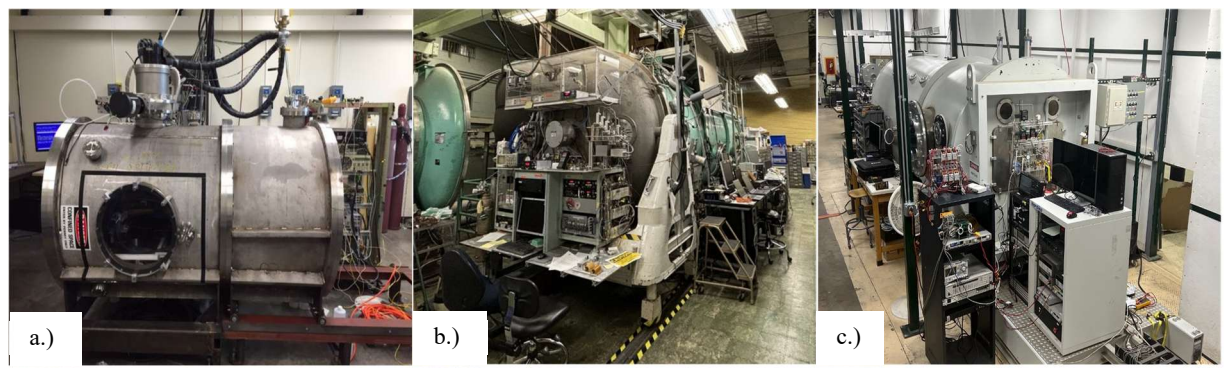


Figure 2. Vacuum test facilities a.) WMU, b.) JPL, & c.) CSU.

C. Diagnostics

The diagnostics used in this investigation, which included an HSRPA and either a Langmuir or an emissive probe, were mounted at thruster centerline height on a three-axis motion stage downstream of the thruster, secured to an 80/20 T-slotted frame. At each spatial location, the diagnostics were aimed directly at the thruster centerline. Plume measurements from three spatial locations are discussed. Figure 3 illustrates the experimental setup utilized in this investigation and provides the exact diagnostic positions that were probed. The green markers represent the measurement locations presented in this work. Results at WMU for position #3 are excluded as the position was not attainable due to the facility size.

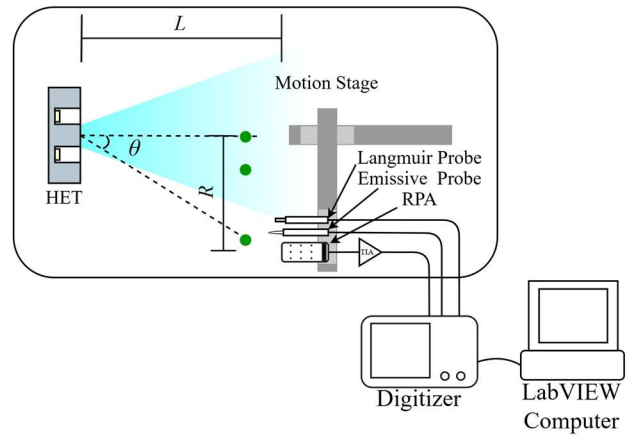


Figure 3. Experimental setup and diagnostic measurement locations.

Table 2. Measurement locations.

	Axial Distance: L	Radial Distance: R	Angle: θ
Position #1	500 mm	0 mm	0°
Position #2	500 mm	165 mm	18°
Position #3	500 mm	487 mm	44°



1. High-Speed Retarding Potential Analyzer

An RPA operates by establishing a variable electric field normal to incoming ions, creating a potential barrier that filters ions with energy lower than the sourced potential. The electric field within an RPA is formed by a series of mesh grids biased to various potentials. The RPA utilized in this study features a four-grid configuration, consisting of three electrostatically biased mesh grids and a floating grid, located upstream of a current collection plate. The body, grids, retention rings, and wires are composed of 316 stainless steel. MACOR washers and a MACOR inner sleeve are used to insulate the grids from the RPA body and each other, while alumina tubing insulates the wires connected to the grids. Figure 4 shows a schematic of the RPA. Grid 1 is floating to minimize disturbance to the plasma from the biased grids and reduce space charge effects inside the diagnostic. Grid 2 is negatively biased to repel plasma-born electrons from entering the RPA. Grid 3 is the retarding grid and is responsible for filtering ions. Grid 4 is biased negatively to suppress secondary electron emission from the grids and collector due to the impact of high-energy ions. The RPA utilized in this investigation possesses an energy resolution, as determined by the geometry of the RPA grids, of approximately 1.5% of the retarding grid potential [13]. Further details on the construction of the RPA can be found in Ref. [14].

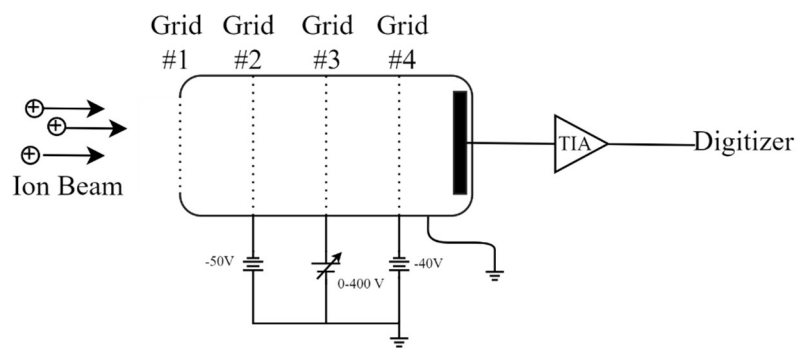


Figure 4. Retarding potential analyzer setup.

A standard RPA operates by sweeping the retarding grid over a range of positive potentials, filtering ions based on their energy per unit charge, E/q. Ions possessing energy exceeding the retarding grid potential can overcome the potential barrier and arrive at the collector, forming a measurable current. By recording the collector current as a function of the retarding potential, an I–V characteristic curve is established. The ion energy distribution function (IEDF) is commonly approximated solely as the negative derivative of the collector current with respect to the retarding grid bias $f(E) \approx -dI_{coll}/V_{bias}$. However, the exact formulation is given by Equation (1),

$$-\frac{dI_{coll}}{dV_{bias}} = Aen_i \sqrt{\frac{2E}{m_i}} f(E).$$
 (1)

The measured IEDF requires correction for the local plasma potential, as the retarding grid of the RPA is ground-referenced. The true ion energy from the RPA is calculated using Equation (2).

$$E = eV_{bias} - eV_p \tag{2}$$

Measurements in this investigation were collected at 150 discrete retarding grid potentials. A Keithley 237 source measurement unit was used to sweep the potential of the retarding grid, while the repelling and suppression grids were biased with a set of batteries to a potential of -50 V and -40 V, respectively. Collector current measurements were converted and amplified using a FEMTO DHPCA-100 commercial TIA. Time-resolved RPA measurements were performed as follows: The retarding grid potential is held constant, as current is collected and sampled at a rate greater than the dynamics being investigated. Simultaneously, a second measurement coupled to the HSRPA collector current measurement is sampled. In this investigation, the coupled measurement is the discharge current of the HET. The retarding grid potential is then increased by the appropriate voltage step size to obtain the desired IEDF resolution. This process is then repeated until a complete distribution is achieved. All time-resolved IEDFs are normalized to the local maximum of the IEDF for each instant in time.



Time-series data reconstruction was performed using a data fusion method known as shadow manifold interpolation (SMI), a non-linear technique based on manifold reconstruction and convergent cross-mapping (CMM), developed by Takens and Sugihara, respectively [15, 16]. Details on SMI and its parameters can be found in Refs [8, 9, 17]. The reconstructed waveforms are then assembled to form I-V curves at each representative point in time. Subsequently, signal noise was reduced by applying a Savitzky–Golay filter to the data after reconstruction and a smoothing spline to the reconstructed I-V curves.

2. Langmuir & Emissive Probe

To facilitate plasma potential measurements, either a Langmuir probe or an emissive probe was utilized. An emissive probe was used at JPL and WMU, while a Langmuir probe was used at CSU, due to a failure of the emissive probe. Langmuir probes provide a simple method to determine plasma properties such as plasma potential, floating potential, ion number density, electron number density, and electron temperature, by analyzing an I-V curve. The I-V curve is obtained by inserting an exposed conductor into a plasma and sweeping the applied potential. A detailed description of Langmuir probe theory and its relevance to electric propulsion can be found in Ref [18]. Emissive probes provide an alternative method for determining plasma potential. In this work, the floating emissive probe with the large emission method was selected for its simplicity. The measurement method and probe construction followed the recommended practices by Sheehan, *et al.* [19, 20]. The plasma potential can be identified by determining where the floating potential of the emissive probe saturates. Each probe provides a reliable determination of plasma potential.

III. Results

The SPT-50 has exhibited variations in discharge characteristics and plume properties in response to changing facility conditions and environmental factors. As observed in previous facility effects investigations with HETs, variations in background pressure, electrical configuration, and impedance pathways have led to alterations in thruster behavior [21–25]. As these factors change between facilities, they are expected to impact the operation and performance of the SPT-50, highlighting the importance of accurately characterizing plume behavior in multiple facilities.

A. Discharge Telemetry

Temporal measurements of thruster telemetry, such as discharge current, provide insight into the role of discharge dynamics in HET operation. Figure 5 shows discharge current traces and power spectral density (PSD) plots for the 200-V, 250-V, and 300-V conditions. All waveform metrics are summarized in Table 4. Additionally, time-averaged cathode-to-ground voltage measurements are presented in Table 3 and can shed light on coupling of electrons to the plume. The time-averaged discharge current reflects the average power draw and the current that flows from the cathode to the anode, while the amplitude of the peak-to-peak oscillations quantify the strength of plasma oscillations, specifically the breathing mode oscillations. By analyzing the frequency spectrum, characteristic oscillation modes linked to physical processes in the discharge can be examined, since periodic oscillations caused by instabilities appear as distinct peaks in the PSD plots.

Inspecting Fig. 5, several differences are apparent between conditions, including variations in the mean, peak-to-peak amplitude, and frequency spectrum of the discharge current. The mean discharge current between all three facilities showed a maximum deviation of 13%, attributed to additional neutral ingestion due to elevated background pressures. Increasing the discharge voltage resulted in a marginal increase in discharge current, amounting to less than 0.1 A. Due to the elevated background pressure, measurements at WMU showed the highest mean discharge current. Significant differences are observed in the amplitude of the peak-to-peak discharge current oscillations and the breathing mode frequency. At all operating conditions, the largest peak-to-peak current amplitude was measured at CSU, with a maximum value of 2.57 A, while the minimum value was measured at JPL at 1.08 A.



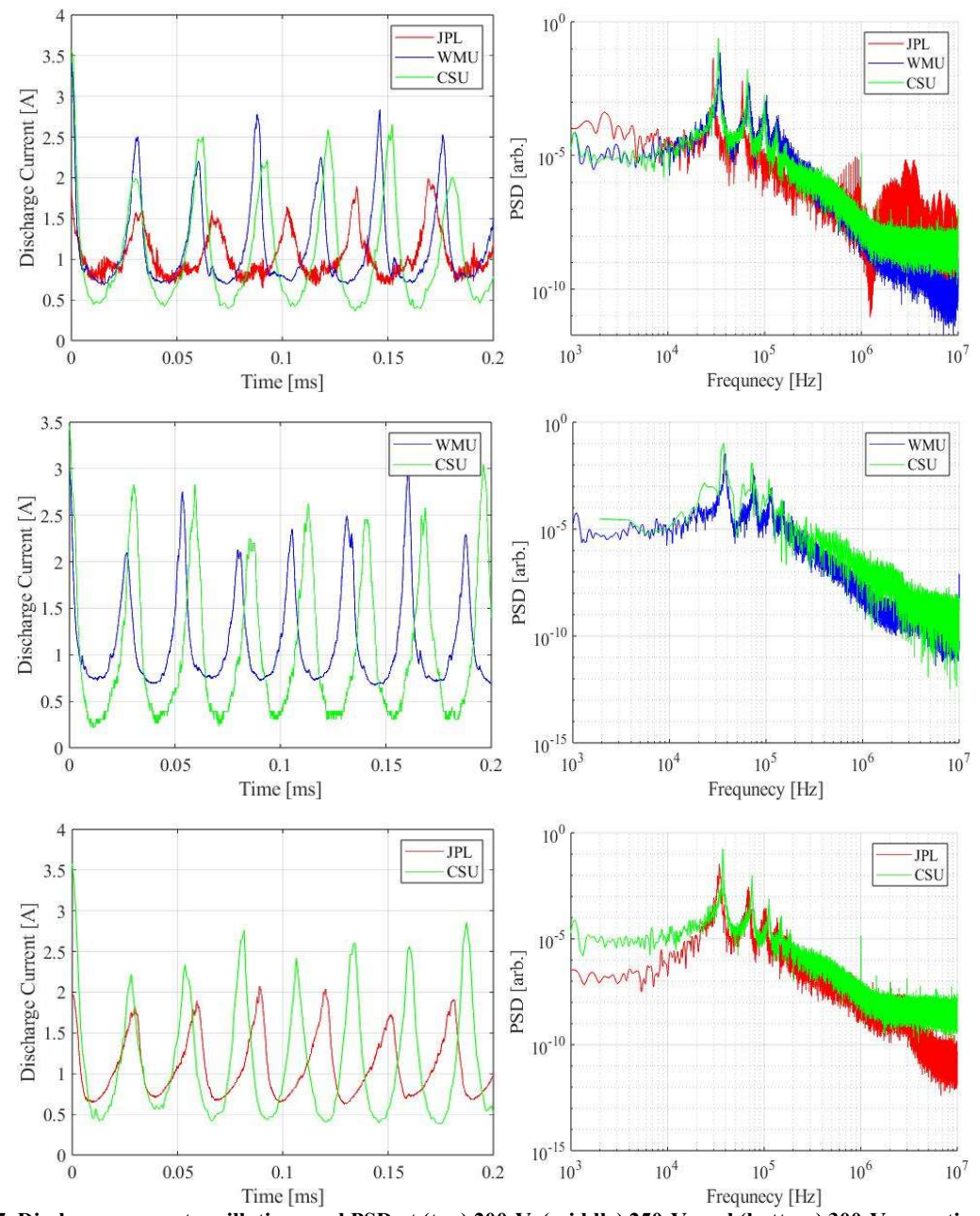


Figure 5. Discharge current oscillations and PSD at (top) 200-V, (middle) 250-V, and (bottom) 300-V operating conditions.



Table 4. Discharge current metrics across tested facilities.

10	Table 4. Discharge current metrics across tested facilities.				
		WMU	CSU	JPL	
	I _{D-avg}	1.16 A	1.01 A	1.05 A	
200 V	I_{D-p2p}	1.91 A	2.54 A	1.08 A	
	f_{BM}	35.1 kHz	32.7 kHz	29.3 kHz	
	I _{D-avg}	1.16 A	1.03 A	N/A	
250 V	I_{D-p2p}	1.80 A	2.57 A	N/A	
	f_{BM}	37.8 kHz	36.0 kHz	N/A	
	I _{D-avg}	N/A	1.09 A	1.10	
300 V	I_{D-p2p}	N/A	2.54 A	1.24	
	f_{BM}	N/A	37.3 kHz	34.5 kHz	

The breathing mode frequency varied by several kilohertz between facilities, with WMU displaying the highest oscillation frequency. The rise in breathing mode frequency likely resulted from a shortening of the ionization and acceleration zones, due to elevated background pressure, leading to a quicker refill time of depleted neutrals [24, 25]. While CSU and JPL have similar operating pressures, a significant difference in frequency is observed; this discrepancy is discussed further in Section IV. The changes in the breathing mode fundamental frequency can be observed in the PSD plots on the right side of Fig. 5. The PSD plots highlight the differences in waveform structure due to changes in the strength of the fundamental frequency and its respective harmonics. Given the similarities between the PSD plots, the thruster appears to have operated in a similar, highly oscillatory mode across facilities and conditions. Section IV considers the influence of facility effects on discharge current metrics and thruster stability.

Table 3. Time-averaged cathode-to-ground voltage across tested facilities.

	WMU	CSU	JPL	
200 V	-9.9 V	-14.9 V	-12.3 V	
250 V	-8.2 V	N/A	N/A	
300 V	N/A	-14.2 V	-12.1 V	

B. Plasma Potential

The time-averaged plasma potential with respect to facility ground, determined by Langmuir or emissive probe measurements, is reported in Table 5. At all facilities, a similar spatial variation was observed, with the highest potentials recorded near the thruster centerline and decreasing with increased transverse position. Higher plasma potentials were also measured at the higher discharge voltage conditions. Plasma potential measurements at CSU consistently showed lower values compared to WMU and JPL. The plasma potential measurements will be used to correct the ion energy measured by the RPA for local plasma potential, as indicated in Equation (2).

Table 5. Plasma potential measurements.

		WMU	CSU	JPL	
200 -	Position #1	$8.7~V\pm1~V$	$5.5~V\pm0.1~V$	$7.7~V\pm1~V$	
200 - V	Position #2	$8.0~V\pm1~V$	$3.2~V\pm0.1~V$	$6.5~V\pm1~V$	
V	Position #3	N/A	$4.3~V\pm0.1~V$	$4.8~V\pm1~V$	
250	Position #1	$9.2~V\pm1~V$	$6.3~V\pm0.1~V$	N/A	
V	Position #2	$8.4~V\pm1~V$	$4.8~V\pm0.1~V$	N/A	
300	Position #1	N/A	$7.4~V\pm0.1~V$	$8.2~V\pm1~V$	
V	Position #2	N/A	$4.3~V\pm0.1~V$	$7.3~V\pm1~V$	



C. Ion Energy

Time-resolved ion energy measurements conducted in different facilities have provided insight into the evolving plasma dynamics within the plume of a low-power HET. Time-resolved IEDFs at the 200-V-condition are shown in Fig. 6, for all three facilities, and the corresponding metrics are summarized in Table 6. A comparison of the IEDFs across facilities reveals both common features and trends in the ion energy dynamics, in addition to facility-specific variations.

At each facility, the primary ion beam population oscillates at its respective breathing mode frequency, with oscillation frequencies differing by up to 6 kHz across facilities. The average ion energy at each facility shows minimal variation, with the largest observed difference being 5 eV between WMU and JPL, while the peak-to-peak ion energy, defined as the range of most probable energies, shows a substantial facility-dependent variation at position #1, with WMU exceeding the other two facilities by approximately 45 eV. The structure or shape of the ion energy waveform at JPL and CSU possesses a strong sinusoidal nature when compared to the time-resolved IEDF at WMU. These differences likely arise from a combination of pressure and electrical configuration effects. Important to note, the measurements made at CSU exhibited strong electromagnetic interference (EMI). As a result, features which appear with moderate probability in the 0 eV -25 eV and 275 eV -300 eV range are believed to be artifacts of the noise and are not part of real ion energy populations.

At position #2, several additional differences emerge. While the primary ion beam population continues to oscillate at or near the breathing mode frequency, additional ion energy populations and waveform features arise. At WMU, charge exchange (CEX) ions and possibly elastically scattered ions appear in the lower energy range of the IEDF. The CEX ions are found in the 0 eV – 25 eV range, while elastically scattered ions appear in the 50 eV – 150 eV range. Each of these populations can be observed oscillating with the breathing mode frequency. These populations are absent from the other facilities, likely due to the lower background pressures and the proximity of the RPA to the vacuum chamber wall. Additionally, at the off-centerline position for WMU, a more sinusoidal structure is observed compared to the centerline measurement. At present, it is unknown as to why the waveform structure becomes more sinusoidal. Inspecting the IEDFs at position #2 for JPL and CSU, which possess similar background pressure and facility size, some major differences arise. At JPL, the IEDF retains its sinusoidal structure, with only minor changes in ion energy characteristics. However, the IEDF measured at CSU loses its sinusoidal structure, and the magnitude of the peak-to-peak ion energy oscillations drops by over 50%. At present, the reason for this result is unknown, but is theorized to have been caused by excessive EMI distorting the lower current signal at the off-centerline positions.

Table 6. Ion energy metrics 200-V-condition.

	Table 6. 100 energy metrics 200-v-condition.				
		WMU	CSU	JPL	
	E _{i-avg}	$166.6 \text{ eV} \pm 3 \text{ eV}$	$169.6 \text{ eV} \pm 3 \text{ eV}$	$171.8 \text{ eV} \pm 3 \text{ eV}$	
Position #1	E_{i-p2p}	$63.4 \text{ eV} \pm 3 \text{ eV}$	$19.4 \text{ eV} \pm 3 \text{ eV}$	$18.4 \text{ eV} \pm 3 \text{ eV}$	
	f_{BM}	35.1 kHz	32.7 kHz	29.3 kHz	
	$E_{i ext{-}avg}$	$174.9 \pm 3 \text{ eV}$	$170.7 \pm 3 \text{ eV}$	$168.0 \text{ eV} \pm 3 \text{ eV}$	
Position #2	E_{i-p2p}	$55.0 \text{ eV} \pm 3 \text{ eV}$	$8.3 \text{ eV} \pm 3 \text{ eV}$	$20.0~eV\pm 3~eV$	
	f_{BM}	34.2 kHz	32.5 kHz	29.2 kHz	
	$E_{i ext{-}avg}$	N/A	$159.9~eV\pm 3~eV$	$162.0 \text{ eV} \pm 3 \text{ eV}$	
Position #3	E_{i-p2p}	N/A	$11.7 \text{ eV} \pm 3 \text{ eV}$	$27.2 \text{ eV} \pm 3 \text{ eV}$	
	f	N/A	32.4 kHz	29.2 kHz	

At position #3, shown in Fig. 7, we begin to observe a broadening of the IEDFs, indicating the presence of additional ion energy populations at JPL and CSU. This is similar to the IEDF at position #2 at WMU. At this position, the IEDF at JPL, Fig. 7a, becomes increasingly distorted, losing some of its sinusoidal structure. The broadening of the IEDF leads to a lower energy population in the 75 eV - 125 eV range. At CSU, Fig. 7b, both a slight sinusoidal oscillation continues to be present along with a similar energy population observed around 100 eV. Artifacts are once again observed in the lower energy range of the IEDF, which are assumed not to be real, due to EMI. The average ion



energy at both facilities drops by approximately 10 eV, while the values of the peak-to-peak oscillations remained relatively constant, varying by only ~3 eV from that measured at position #2.

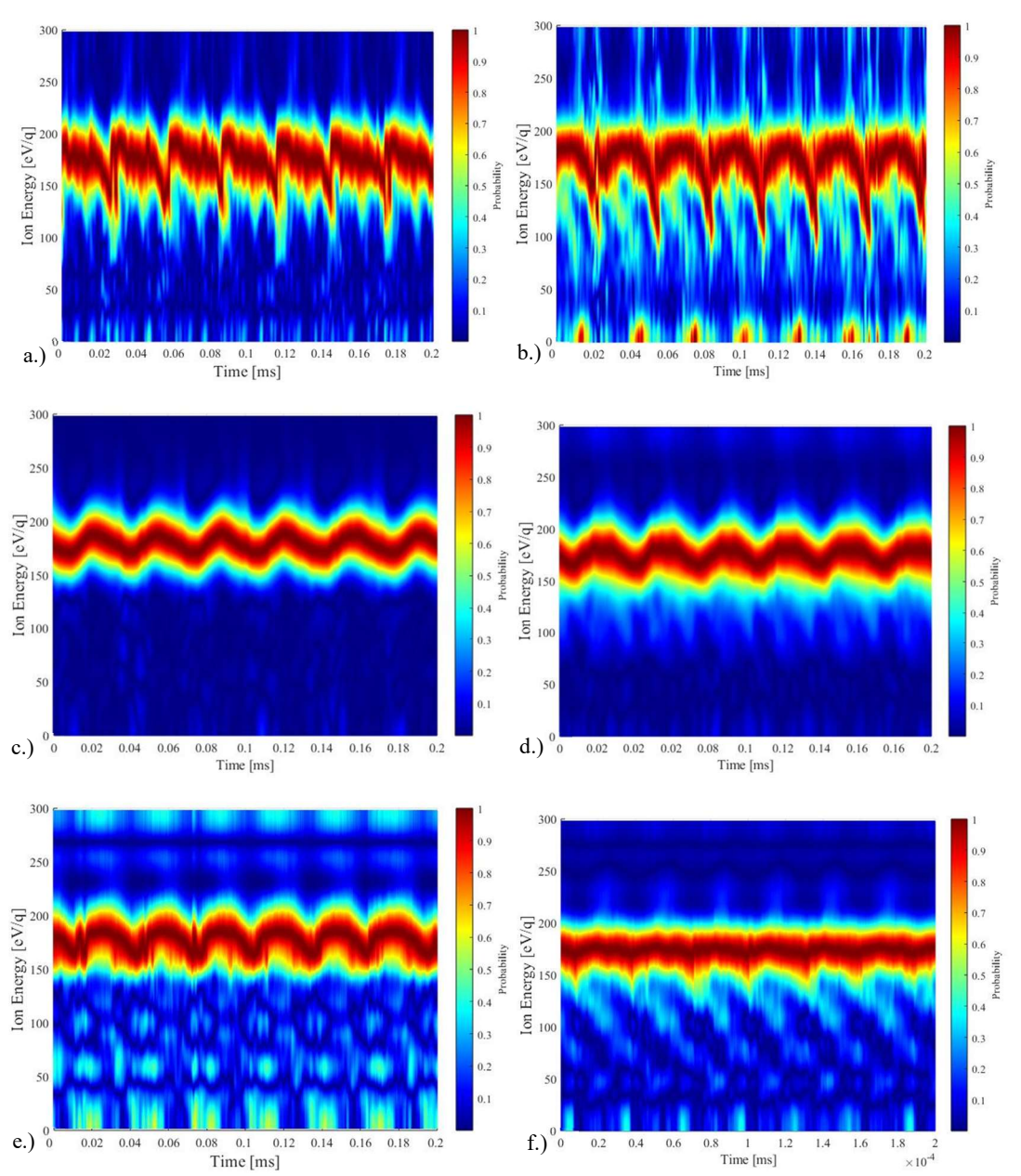


Figure 6. Time-resolved IEDFs 200-V-condition a.) WMU — Position #1, b.) WMU — Position #2, c.) JPL — Position #1, d.) JPL — Position #2, e.) CSU — Position #1, & f.) CSU — Position #2.



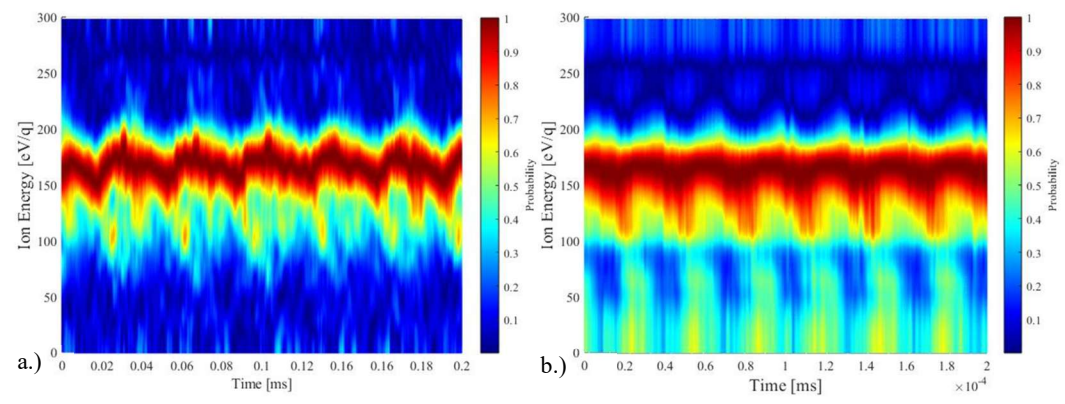


Figure 7. Time-resolved IEDFs 200-V-condition position #3 at a.) JPL and b.) CSU.

Figure 8 shows the IEDFs for the 250-V-condition for WMU and CSU. At positions #1 and #2, the IEDFs for both facilities share similarities with the 200-V-condition. At WMU, the IEDF transitions from a distorted square-wave structure measured at the thruster centerline to a cleaner oscillation, with sine-wave–like features, and a more constant energy holding at ~230 eV at the off-centerline position. At CSU, the same trends observed at the 200-V-condition are replicated. Position #1 exhibits a strong sinusoidal waveform, while position #2 appears more random and loses its sinusoidal structure. At both facilities, the breathing mode frequency increases at a minimum by 2 kHz compared to the 200-V-condition, as expected for an increase in discharge voltage [26–28]. Table 7 presents the ion energy metrics for the 250-V-condition. Changes in both the ion energy mean and magnitude of the peak-to-peak oscillations of the ion energy are observed in the IEDFs at WMU between Position #1 and Position #2. However, at CSU, these metrics remained constant within the energy resolution of the RPA used in this investigation. The mean ion energy at both facilities and positions increased with the higher discharge voltage, as expected, while the magnitude of the peak-to-peak oscillations in the ion energies decreased. Additionally, CEX ions are clearly observed in the 0 eV – 25 eV range at WMU, with no such populations believed to be present at CSU.

Table 7.	Ion	energy	metrics	250-	-V-	condition.
----------	-----	--------	---------	------	-----	------------

		WMU	CSU
	E _{i-avg}	$217.8 \text{ eV} \pm 3.7 \text{ eV}$	$220.6 \text{ eV} \pm 3.7 \text{ eV}$
Position #1	E_{i-p2p}	$38.2 \text{ eV} \pm 3.7 \text{ eV}$	$10.5 \text{ eV} \pm 3.7 \text{ eV}$
	f_{BM}	37.2 kHz	36.4 kHz
	E _{i-avg}	$223.6 \text{ eV} \pm 3.7 \text{ eV}$	$218.2 \text{ eV} \pm 3.7 \text{ eV}$
Position #2	E_{i-p2p}	$22.6 \text{ eV} \pm 3.7 \text{ eV}$	$10.0 \text{ eV} \pm 3.7 \text{ eV}$
	f_{BM}	37.6 kHz	36.4 kHz



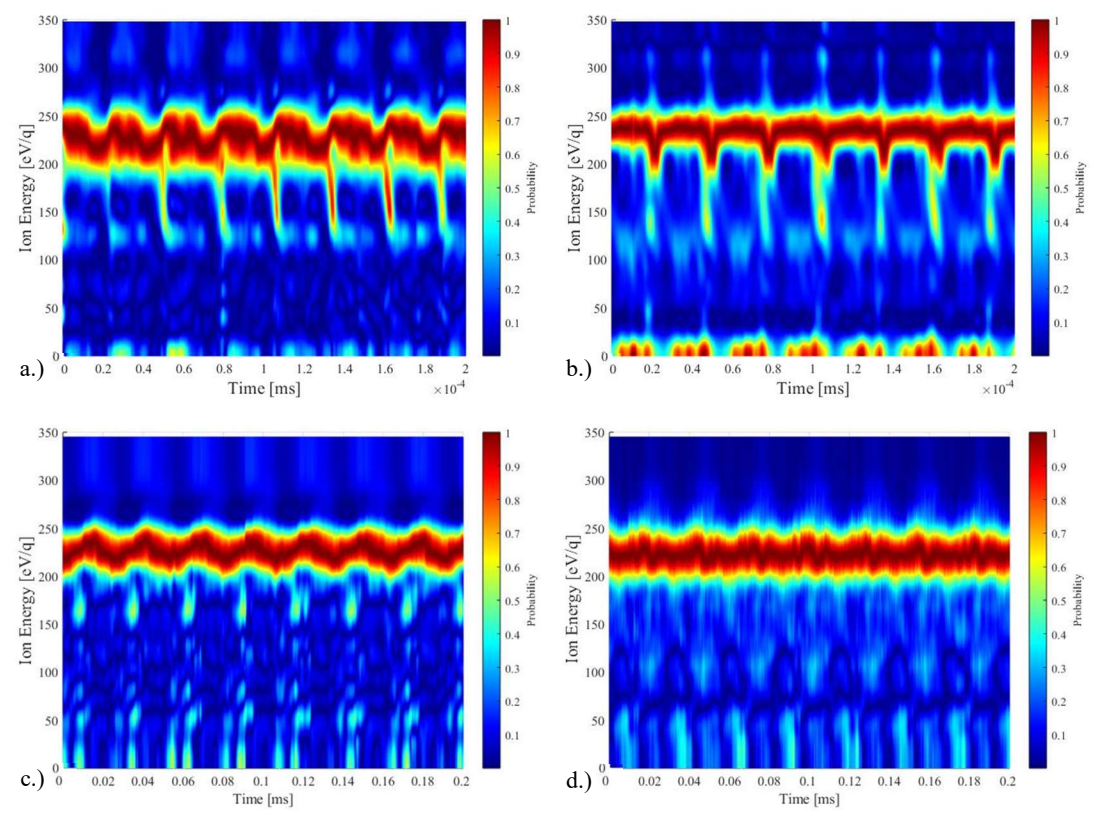


Figure 8. Time-resolved IEDFs 250-V-condition a.) WMU — Position #1, b.) WMU — Position #2, c.) CSU — Position #1, & d.) CSU — Position #2.

The time-resolved IEDFs for the 300-V-condition are shown Fig. 9. As with the previous operating conditions, the mean ion energies are shifted in proportion to the discharge voltage. At this condition, however, the IEDFs at CSU appear significantly distorted, showing little oscillatory nature, compared to the measurements at JPL, which show a strong sinusoidal waveform at both the centerline and off-centerline positions. The ion energy metrics for the 300-V-condition are shown in Table 8.

Table 8. Ion energy metrics 300-V-condition.

	<u> </u>	CSU	JPL
	E_{i-avg}	$268.3 \text{ eV} \pm 4.5 \text{ eV}$	268.0 eV eV ± 4.5 eV
Position #1	E_{i-p2p}	$8.0 \text{ eV eV} \pm 4.5 \text{ eV}$	56.0 eV eV ± 4.5 eV
	f_{BM}	32.3 kHz	34.2 kHz
	E_{i-avg}	$268.6 \text{ eV eV} \pm 4.5 \text{ eV}$	$260.0 \text{ eV eV} \pm 4.5 \text{ eV}$
Position #2	E_{i-p2p}	$8.8 \text{ eV} \text{ eV} \pm 4.5 \text{ eV}$	$44.0 \text{ eV} \text{ eV} \pm 4.5 \text{ eV}$
	f_{BM}	32.3 kHz	32.6 kHz



Measurements at JPL showed an increase in the magnitude of the peak-to-peak ion energy oscillations with increasing discharge voltage, while at CSU ion energy oscillations appeared to be attenuated with increasing discharge voltage. This attenuation is observed across all discharge voltage conditions measured at CSU. One possible explanation is that higher discharge voltages led to increased EMI, resulting in the severely distorted IEDFs. The IEDFs at CSU for the 300-V-condition also contain low and high-energy artifacts. While it is possible that these features represent true behavior at the CSU facility, this is unlikely given that no major changes were observed in the thruster discharge telemetry between operating conditions.

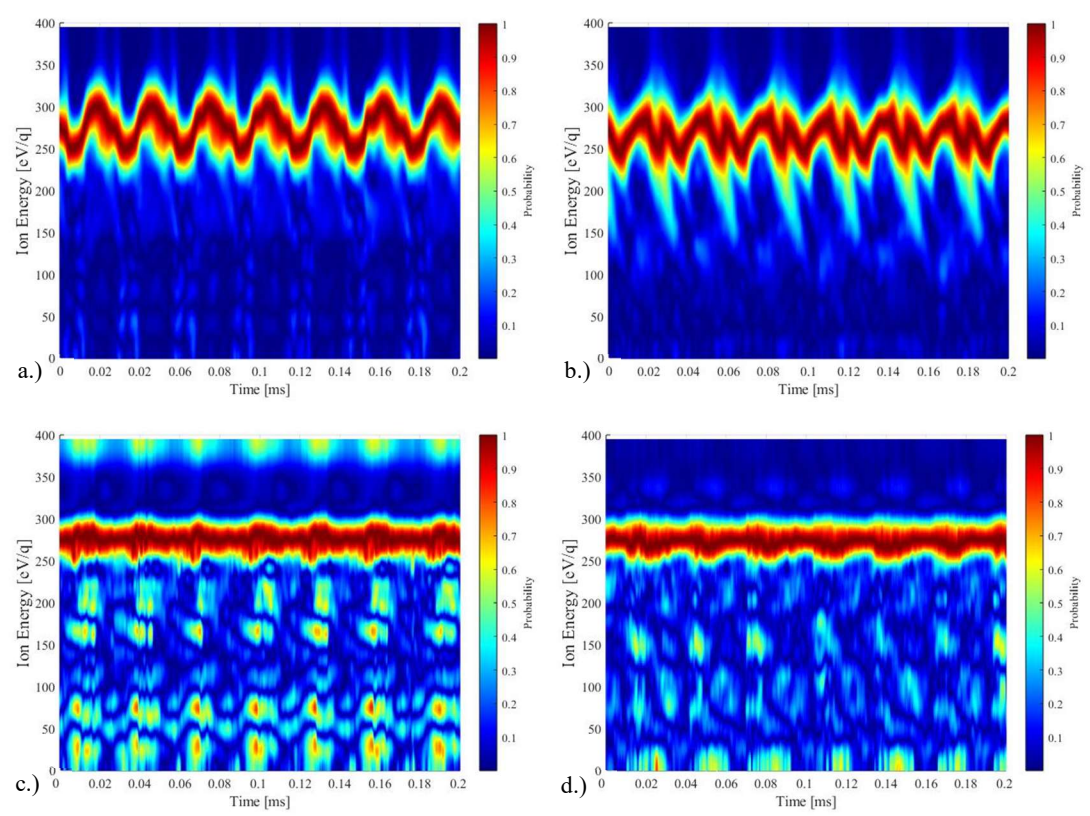


Figure 9. Time-resolved IEDFs 300-V-condition a.) JPL — Position #1, b.) JPL — Position #2, c.) CSU — Position #1, & d.) CSU — Position #2.

IV. Discussion

The above results compare discharge telemetry and plume measurements from three vacuum facilities, in an effort to quantify the impact of facility conditions on HET operation. Discharge current telemetry was recorded at each facility for up to three discharge voltage operating conditions. Variations in discharge current mean, peak-to-peak amplitude, and oscillation frequency were observed across the facilities. These variations between facilities can be the result of several factors, including but not limited to background pressure, cathode position, and operating mode [29–33]. In this study, a combination of these factors is believed to have contributed to the changes observed. With increases in background pressure, the mean discharge current and the breathing mode frequency rose. Given the similar background pressures at JPL and CSU, the expected difference in breathing mode frequency should be minor. However, differences reached as high as 3.5 kHz. A possible explanation for this variation is that, despite efforts to maintain consistent cathode positioning, the radial position of the cathode may have differed between facilities by as much as 1 cm. Walker et al. has shown that cathode position can affect both the fundamental frequency of the breathing mode and the magnitude of the peak-to-peak oscillations of the discharge current [32].



Trends in peak-to-peak discharge current with background pressure have shown conflicting reports; both increasing and decreasing peak-to-peak current have been observed with rising background pressure [29, 30, 34]. In this work, no clear trend was observed. Between JPL and CSU, the magnitude of the oscillations of the discharge current varied by a maximum of 1.46 A at the 200-V-condition. Given that these facilities possess similar pressures, it is unlikely this large variation was caused by increased neutral ingestion and is more likely the result of cathode operation. It is important to note, the cathode tip was replaced after testing at JPL concluded. The replacement of the tip could have led to a greater emission current from the cathode at the WMU and CSU facilities.

Inspecting the PSDs from Fig. 5 provides some indication of the stability of the thruster operating in the different facilities. With pressure as the primary driver of discharge current variations, WMU would be expected to exhibit the least stable operation, as it operates at the highest pressure. Previous studies have shown that higher background pressure leads to reduced stability [34, 35]. At the 200-V-condition, the PSD results partially support this assumption, showing the most broadband behavior in both the fundamental frequency and its harmonics. However, a less stable system is generally accompanied by greater oscillation magnitudes in the discharge current, appearing as a higher magnitude in the PSD. In this work, CSU displayed the largest oscillations but appeared the most stable, with JPL and WMU showing progressively greater harmonic amplitude and broadband behavior. Further testing is required to confirm the primary driver of thruster stability.

Expected trends were observed in the plasma potential measurements which ranged between 3.2 V - 9.2 V across all facilities. The maximum measured values occurred at centerline locations and the minimum at the greatest transverse distance. In regions where the electron temperature is expected to be lower, such as farther downstream and at greater traverse locations, lower plasma potentials are observed [36]. Between facilities for a given position and operating condition, a larger spread was observed than anticipated, reaching a maximum of 3.3 V. The plume properties, such as plasma potential, are significantly affected by background pressure, due to a reduction in electron energy, caused by increased electron-neutral collisions within the plume or a reduction in the cathode potential [25, 37]. As such, it was expected that the plasma potential would be lower at WMU. However, observations at WMU consistently showed the greatest plasma potential measurements when measured with respect to ground. If instead, we take plasma potential measurements with respect to cathode potential, the measurements are shifted and show that the lowest plasma potentials are found at WMU, while JPL and CSU show good agreement. The estimated Langmuir probe uncertainty was 0.1 V. Floating emissive probe measurements typically underestimate the plasma potential between $1.5T_e/e$ and $2T_e/e$ [20]. At the measurement locations performed in this work, T_e is typically on the order of $\sim 1 \text{ eV}$, resulting in a relatively small error of no more than 2 V [38].

Time-resolved ion energy measurements across the three facilities and operating conditions displayed varying ion energy characteristics. While time-averaged ion energy measurements produced consistent results, several temporal ion energy characteristics, including the magnitude of the ion energy oscillations and the waveform structure, showed unexpected behavior. Two factors are considered as possible contributors to these differences: background pressure and the facility electrical configuration.

Literature discusses the impact of background pressure on time-averaged ion energy extensively [23, 25, 37]. Increased background pressure results in the broadening of the energy distributions due to additional CEX ions being measured in the plume and causes a minor reduction in the most probable ion energy. Extending these effects to the temporal ion energy, greater peak-to-peak ion energies are expected at higher pressures, possibly resulting from ions being born at lower acceleration potentials, movement of the acceleration region, or CEX collisions within the channel and plume. Figure 6 supports this result. At WMU, the average most probable ion energy was lowest by approximately 5 eV, and the ion energy oscillation magnitude was higher at both positions compared to JPL and CSU. The higher background pressure also resulted in additional ion energy populations not observed at JPL and CSU, including elastically scattered and CEX ions. These populations possessed the temporal characteristics of the discharge, oscillating at the breathing mode frequency. Similar trends are observed at the 250-V-operating condition when compared between WMU and CSU.

Figure 7 shows the IEDFs for position #3 for JPL and CSU. Here, a broadening of the IEDFs is observed, possibly resulting from CEX ions being born within the channel and experiencing only part of the acceleration potential. It is also possible that these are elastically scattered ions, as their energies fall within the range expected for populations



that have experienced energy loss due to elastic collisions. The energy of an ion that undergoes an ideal elastic collision and is scattered at an angle θ by another ion initially at rest is proportional to $Ecos^2(\theta)$ [36]. At the measurement location within the plume, with an angle of 44° relative to the thruster centerline and given the large acceptance half-angle of the RPA used in this study of 20°, the measured energies fall within this range. However, while the energies agree with what is seen in the IEDFs, given the background pressure and distance of the RPA within the plume, elastic collision mean free paths are on the order of 1 m, which suggests that elastic collisions are not the dominant mechanism. These IEDFs also possess the temporal characteristics of the primary discharge. A potential CEX ion population was observed in Fig. 7b. However, as stated in Section III, measurements made at CSU experienced high levels of EMI; as such, several artifacts are present within the IEDFs. This population is believed not to be real and is instead a result of I-V curve distortion of the low current signal. These artifacts are also present in the remaining IEDFs measured at CSU.

Between facilities, operating conditions, and positions, the IEDFs waveform structure differs drastically. The structure of the IEDF waveform is believed to be the result of both pressure and electrical facility effects. Changes in the background pressure can impact collision rates, resulting in the generation of various ion energy populations and affecting the ionization and acceleration zones, as discussed above. The facility electrical configuration, including its power supplies, harnessing, and discharge filter, can also influence the voltage measured at the anode [39–41]. Fluctuations in anode voltage are thought to play a role in the IEDF structure. Typical anode voltage fluctuations are only on the order of 1 V, much lower than the ion energy oscillations observed in this study; however, these oscillations can grow depending on the electrical properties of the harness, particularly its inductance [39]. While voltage fluctuations can directly impact the ion energy oscillations, it is hypothesized that the ion energy oscillations observed in an IEDF are influenced by a combination of background pressure and the voltage at the anode. As the 200-V and 300-V-operating conditions for JPL and CSU were conducted under similar background pressures for facilities of similar size, it is assumed that the electrical configuration plays a non-negligible role in influencing the IEDF. Results on the influence of the facility electrical configuration will be presented in future work.

This investigation has highlighted some of the potential consequences of testing at different facilities and the factors that could influence the operation of an HET. The data are intended to be used to calibrate a PEM for the SPT-50. Although the plasma dynamics and properties vary between low-powered and high-powered HETs, the core principles governing their operation remain unchanged. Trends could be extrapolated from the operation of the SPT-50 facility testing to higher power operation in facilities with higher pumping capacity. At present, data have been provided to initiate the development of a PEM for the SPT-50 and testing at a fourth facility has been completed.

V. Conclusion

A facility characterization study was performed on the SPT-50 across three vacuum facilities. The results showed variations in discharge telemetry and plume measurements, revealing the influence of facility conditions on HET operation. Background pressure was observed to affect the performance, stability, and plume properties of an HET, consistent with previous reports. Discharge telemetry showed variations in mean current, the peak-to-peak amplitude, and oscillation frequency, while time-averaged plume properties displayed variations in magnitude and energy profile. Temporal ion energy characteristics, such as waveform structure and the peak-to-peak amplitude, demonstrated sensitivity to both pressure and potentially, facility electrical configuration. The data obtained in this investigation will be used for the development of a low-power HET PEM.

Acknowledgments

This work was partially supported by NASA through the Joint Advanced Propulsion Institute, a NASA Space Technology Research Institute, grant number 80NSSC21K1118

References

¹ Wirz, R., Gorodetsky, A., Jorns, B., & Walker, M. *Predictive Engineering Model for Life and Performance Assessment of High-Power Electric Propulsion Systems*. Presented at the 37th International Electric Propulsion Conference. Massachusetts Institute of Technology, Cambridge, MA USA. 2022.



- ²Walker, M., Lev, D., Saeedifard, M., Jorns, B., Foster, J., Gallimore, A., Gorodetsky, A., Rovey, J., Chew, H., Levin, D., Williams, J., Yalin, A., Wirz, R., Marian, J., Boyd., I., Hara, K., & Lemmer, K. *Overview of the Joint AdvaNced PropUlsion InStitute (JANUS)*. Presented at the 37th International Electric Propulsion Conference. Massachusetts Institute of Technology, Cambridge, MA USA. 2022.
- ³Eckels, J., Marks, T., Allen, M., Jorns, B., & Gorodetsky, A. "Hall Thruster Model Improvement by Multidisciplinary Uncertainty Quantification." *Journal of Electric Propulsion*, vol. 3, no. 1, 2024, p. 19, https://doi.org/10.1007/s44205-024-00079-w
- ⁴Lobbia, R., Gallimore, A. "High-Speed Dual Langmuir Probe." *Review of Scientific Instruments*, vol. 81, no. 7, 2010, pp. 073503-073503-09, https://doi.org/10.1063/1.3455201.
 - ⁵Lobbia, R. Time-resolved Investigation of the Hall Thruster Breathing Mode. Ph.D thesis, University of Michigan, 2010.
- ⁶Durot, C. Development of a Time-Resolved Laser-Induced Fluorescence Technique for Nonperiodic Oscillations. Ph.D thesis, University of Michigan, 2016.
- ⁷Durot, C., Gallimore, A., & Smith, T. "Validation and Evaluation of a Novel Time-Resolved Laser-Induced Fluorescence Technique." *Review of Scientific Instruments*, vol. 85, no. 1, 2014, p. 013508, https://doi.org/10.1063/1.4856635.
- ⁸Baird, M., McGee-Sinclair, R., Lemmer, K., & Huang, W. "Time-resolved ion energy measurements using a retarding potential analyzer". *Review of Scientific Instruments*, vol. 92, no. 7, Jul. 2021, doi: 10.1063/5.0039621.
- ⁹Thomas, A. & Lemmer, K. "Time-resolved Ion Energy Measurements Using a Retarding Potential Analyzer for Electric Propulsion Applications". *Rev. Sci. Inst.*, 1 February 2024; 95 (2): 023505. https://doi.org/10.1063/5.0176167
- ¹⁰Choueiri, E. "Plasma Oscillations in Hall Thrusters." *Physics of Plasmas*, vol. 8, no. 4, 2001, pp. 1411–26, https://doi.org/10.1063/1.1354644.
- ¹¹Clauss, C., Tilley, D., & Barnhart, D. "Benefits of Low-Power Stationary Plasma Thruster Propulsion for Small Satellites". 1995.
- ¹²Manzella, D., Oleson, S., Sankovic, J., Hagg, T., Semenkin, A., & Kim, V. "Evaluation of Low Power Hall Thruster Propulsion". Presented at the 32nd Joint Propulsion Conference, 1996.
- ¹³Enloe, C. "High-resolution retarding potential analyzer, Review of Scientific Instruments". vol. 65, no. 2, pp. 507–508, 1994, doi: 10.1063/1.1145167.
- ¹⁴Baird, M., Kerber, T., Lemmer, K., Huang W. "Hall Thruster Plume Measurements of Time Resolved Ion Energy". Presented at the 36th International Electric Propulsion Conference, 2019.
 - ¹⁵Takens, F. "Detecting strange attractors in turbulence". 1981, pp. 366–381. doi: 10.1007/bfb0091924.
- ¹⁶Sugihara, G., May, R., Ye, H., Hsieh, C., Deyle, E., Fogarty, M., & Munch, S." Detecting Causality in Complex Ecosystems". *Science (American Association for the Advancement of Science)*, 338(6106), 496–500. 2012. https://doi.org/10.1126/science.1227079
- ¹⁷Eckhardt, D., Koo, J., Martin, R., Holmes, M., & Hara, K. "Spatiotemporal data fusion and manifold reconstruction in Hall thrusters". *Plasma Sources Sci Technol*, vol. 28, no. 4, Apr. 2019, doi: 10.1088/1361-6595/ab0b1f.
- ¹⁸Lobbia, R. & Beal B. "Recommended practice for use of Langmuir probes in electric propulsion testing". *Journal of Propulsion and Power, vol. 33, no. 3, 2017, pp. 566–81, https://doi.org/10.2514/1.B35531.*
- ¹⁹Sheehan, J. and Hershkowitz, N. Emissive probes. *Plasma Sources Science & Technology*, 20(6), 063001-1–22. 2011. https://doi.org/10.1088/0963-0252/20/6/063001
- ²⁰Sheehan, J., Raitses, Y., Hershkowitz, N., and McDonald, M. "Recommended practice for use of emissive probes in electric propulsion testing", 2017, *American Institute of Aeronautics and Astronautics Inc.* doi: 10.2514/1.B35697.
- ²¹Walker, J., Langendorf, S., Walker, M., Khayms, V., King, D., & Peterson P. (2016). "Electrical facility effects on hall current thrusters: Electron termination pathway manipulation". *Journal of Propulsion and Power*, 32(6):1365–1377. https://doi.org/10.2514/1.B35904
- ²²Jovel, D., Cabrera, J., & Walker, M. "Current Pathways Model for Hall Thruster Plumes in Ground-Based Vacuum Test Facilities: Measurements and Observations". *Journal of Electric Propulsion*, vol. 3, no. 1, 2024, p. 35, https://doi.org/10.1007/s44205-024-00097-8.
- ²³Huang, W., Kamhawi, H., & Haag, T." Effect of Background Pressure on the Performance and Plume of the HiVHAc Hall Thruster". Presented at the 33rd International Electric Propulsion Conference. Washington University, Washington, D.C., USA. 2013.
- ²⁴Huang, W., Kamhawi, H., Lobbia, R., & Brown, D. "Effect of Background Pressure on the Plasma Oscillation Characteristics of the HiVHAc Hall Thruster". *50th AIAA/ASME/SAE/ASEE Joint Propulsion Conference, Cleveland, OH, July 28-30, 2014*, American Institute of Aeronautics and Astronautics, 2014, pp. 1–1.
- ²⁵Diamant, K., Curtiss, T., Spektor, R., Beiting, E., Hruby, V., Pote, B., Kolencik, J., & Paintal, S. Performance and Plume Characterization of the BHT-1500 Hall Thruster. Presented at Joint Conference of 30th International Symposium on Space



- $Technology \ and \ Science \ 34th \ International \ Electric \ Propulsion \ Conference \ and \ 6th \ Nano-satellite \ Symposium, \ Hyogo-Kobe, \ Japan \ July \ 4-10, \ 2015$
- ²⁶Baird, M., Kerber, T., McGee-Sinclair, R,. & Lemmer, K. "Plume Divergence and Discharge Oscillations of an Accessible Low-Power Hall Effect Thruster." *Applied Sciences*, vol. 11, no. 4, 2021, p. 1973, https://doi.org/10.3390/app11041973.
- ²⁷Xia, G., Liu, X., Li, H., Ding, Y., Wei, L., Chen, S., & Yu, D., "Performance Improvement of Hall Thrusters with High Discharge Voltage." *Vacuum*, vol. 172, 2020, p. 109052, https://doi.org/10.1016/j.vacuum.2019.109052.
- ²⁸Y. Azziz. "Experimental and Theoretical Characterization of a Hall Thruster Plume." Ph.D thesis, Massachusetts Institute of Technology, (2007).
- ²⁹Snyder, J., Lenguito, G., Frieman, J., Haag, T., & Mackey, J. "Effects of Background Pressure on SPT-140 Hall Thruster Performance." *Journal of Propulsion and Power*, vol. 36, no. 5, 2020, pp. 668–76, https://doi.org/10.2514/1.B37702
- ³⁰Kamhawi, H., Huang, W., Haag, T., Shastry, R., Thomas, R., Yim, J., Herman, D., Williams, G., Myers, J., Hofer, R., Mikellides, I., Sekerak, M., & Polk, J. "Performance and Facility Background Pressure Characterization Tests of NASA's 12.5-kW Hall Effect Rocket with Magnetic Shielding Thruste"r. Presented at Joint Conference of 30th International Symposium on Space Technology and Science 34th International Electric Propulsion Conference and 6th Nano-satellite Symposium, Hyogo-Kobe, Japan July 4 10, 2015
- ³¹Frieman, J., Walker, J., Walker, M., Khayms, V., & King, D. "Electrical Facility Effects on Hall Thruster Cathode Coupling: Performance and Plume Properties." *Journal of Propulsion and Power*, vol. 32, no. 1, 2016, pp. 251–64, https://doi.org/10.2514/1.B35683.
- ³²Walker, J., Frieman, J., Walker, M., Khayms, V., King, D., & Peterson, P. "Electrical Facility Effects on Hall-Effect-Thruster Cathode Coupling: Discharge Oscillations and Facility Coupling." *Journal of Propulsion and Power*, vol. 32, no. 4, 2016, pp. 844–55, https://doi.org/10.2514/1.B35835.
- ³³Brown, Daniel L., & Alec D. Gallimore. *Investigation of Low Discharge Voltage Hall Thruster Operating Modes and Ionization Processes*. Presented at the 31st International Electric Propulsion Conference, University of Michigan, Ann Arbor, Michigan, USA September 20 24, 2009 op
- ³⁴Diamant, K., Spektor, R., Beiting, E., Young, J., & Curtiss, T. "The Effects of Background Pressure on Hall Thruster Operation." 48th AIAA/ASME/SAE/ASEE Joint Propulsion Conference & Exhibit, 30 July 2012 01 August 2012, Atlanta, Georgia, American Institute of Aeronautics and Astronautics (AIAA), 2012, pp. 1–1.
- ³⁵Kamhawi, H., Huang, W., Haag, T., Yim, J., Herman, D., Peterson, P., Williams, G., Gilland, J., Hofer, R., & Mikellides, I. "Performance, Facility Pressure Effects, and Stability Characterization Tests of NASA's Hall Effect Rocket with Magnetic Shielding Thruster." *52nd AIAA/SAE/ASEE Joint Propulsion Conference, Salt Lake City, UT, July 25-27, 2016*, American Institute of Aeronautics and Astronautics, 2016, pp. 1–2.
 - ³⁶Goebel, D., Katz, I., & Mikellides, I. Fundamentals of Electric Propulsion: Ion and Hall Thrusters. 2nd ed., Wiley, 2023.
- ³⁷Diamant, K., Liang, R., & Corey, & R. "The Effect of Background Pressure on SPT-100 Hall Thruster Performance." *50th AIAA/ASME/SAE/ASEE Joint Propulsion Conference, Cleveland, OH, July 28-30, 2014*, American Institute of Aeronautics and Astronautics (AIAA), 2014, pp. 1–1.
- ³⁸Dannenmayer, K., Kudrna, P., Tichý, M., & Mazouffre, S. "Measurement of Plasma Parameters in the Far-Field Plume of a Hall Effect Thruster." *Plasma Sources Science & Technology*, vol. 20, no. 6, 2011, pp. 65012-1–9, https://doi.org/10.1088/0963-0252/20/6/065012.
- ³⁹Pinero, L. "The Impact of Harness Impedance on Hall Thruster Discharge Oscillations". Presented at the 35th International Electric Propulsion Conference. Georgia Institute of Technology Atlanta, GA USA. 2017
- ⁴⁰Brieda, L., Koo, J., and Scharfe, M. "Influence of a power supply model on simulated Hall thruster discharge voltage oscillations". *AIP Adv*, vol. 9, no. 2, Feb. 2019, doi: 10.1063/1.5063440.
- ⁴¹Krishnan, A., Lev, D., Saeedifard, M., Graber, L., & Walker, M. "Impedance Analysis of the Hall Thruster Discharge Circuit and Plasma Load to Address Harness Facility Effects." *Presented at the 38th International Electric Propulsion Conference (IEPC-2024-619)*, 23–28 June 2024, Toulouse, France.

